interpretation of the tractography models, which highlighted different features of the fiber architecture, adding valuable information of existent muscular layers. In order to further clarify the anatomic characterization, we applied multiresolution models that build different models of the same data with different levels of detail without losing fidelity. This technique is based on the well-known pyramid representation (6), which applies a Gaussian filtering and subsequent exponential reduction via a subsampling of the full-scale information. Reduced information is a summary of the original and would be used to represent it at different scales. This technique can be applied to the DT-CMR dataset in order to simplify its complexity. By downscaling 2 orders of magnitude of the original sets and applying our streamlining, we got a simplified tractography (Fig. 1). Comparing it to the full-scale tractography, also shown in Figure 1, it is easy to notice that the simplified one keeps the main geometric features of the fibers.

The simplified tractographic reconstruction method (Fig. 1) showed a continuous helical structure of the ventricular myocardium, tracked from the pulmonary artery (PA) to the aorta (Ao). The helical structure enclosing the basal ring can be further tracked inside the left ventricle toward the apex and is seen to orient in counterdirectional helical orientations around the ventricles. To further simplify the backbone myocardial fiber spatial orientation, we explored the geometry of the heart by looking for long paths that can represent connected regions on the DT-CMR tractography. The goal of this procedure was to provide a comprehensive reconstruction allowing interpretation at first sight by any possible observer. By manually picking seeds at the basal level, we resolved continuous paths connecting both ventricles. Figure 2 shows 4 tracts of simplified models reconstructed from manually picked seeds located at the basal level near the PA. We observe that the tracts define a sample-wide coherent helical structure for all canine samples. The use of visualizations with single tracts changes the way in which this structure can be viewed.

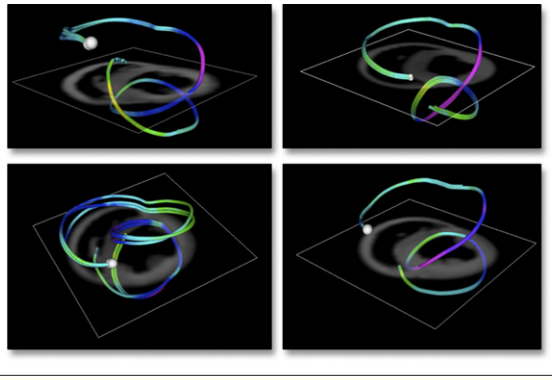

Figure 2. Selected Paths Highlighting the Helical Structure of the Myocardium

Example of tracts reconstructed with manually picked seeds, always chosen near the pulmonary artery, on simplified tractography.

Our reconstructions support a helical ventricular myocardial fiber array from a complete set of local evidence and also from a global automated reconstruction of the myocardial structure.

Acknowledgments

The authors want to acknowledge Drs. Patrick A. Helm and Raimond L. Winslow at the Center for Cardiovascular Bioinformatics and Modeling and Dr. Elliot McVeigh at the National Institutes of Health for provision of datasets of DT-CMR.

Ferran Poveda, MSc,* Enric Martí, PhD, Debora Gil, PhD, Francesc Carreras, MD, Manel Ballester, MD, PhD

*DCC Departament de Ciències de la Computació (UAB), IAM Interactive and Augmented Modelling Group (CVC), Universitat Autònoma de Barcelona, 08193 Bellaterra, Barcelona, Catalonia, Spain. *E-mail: ferran.poveda@uab.cat*

http:dx.doi.org/10.1016/j.jcmg.2012.04.005

Please note: This work was supported by the Spanish projects PI071188, TIN2009-13618, and CSD2007-00018. Dr. Gil has been supported by the Ramon y Cajal Program.

REFERENCES

1. Torrent-Guasp F, Ballester M, Buckberg G, et al. Spatial orientation of the ventricular muscle band: physiologic contribution and surgical implications. J Thorac Cardiovasc Surg 2001;122:389–92.
2. Anderson R, Ho S, Redmann K, Sanchez-Quintana D, Lunkenheimer P. The anatomical arrangement of the myocardial cells making up the ventricular mass. Euro J Cardiothorac Surg 2005;28:517–25.
3. Scollan DF, Holmes A, Winslow R, Forder J. Histological validation of myocardial microstructure obtained from diffusion tensor magnetic resonance imaging. Am J Physiol 1998;275:H2308–18.
4. Granger RA. Fluid Mechanics. New York, NY: Courier Dover Publications, 1995.
5. Fehlberg E. Klassische Runge-Kutta-Formeln vierter und niedrigerer ordnung mit schrittweiten-kontrolle und ihre anwendung auf wärmeleitungsprobleme. Computing (Arch Elektron Rechnen) 1970;6:61–71.
6. Burt P. Fast filter transform for image processing. Comput Graph Image Process 1981;16:20–51.

Defining the Diagnosis in Echocardiographically Suspected Senile Systemic Amyloidosis

Senile systemic amyloidosis (SSA) is a cardiomyopathy mainly affecting elderly men due to intramyocardial deposition of wild-type (nonmutant) transthyretin (TTR) (1). Since the heart is the only involved organ, SSA—which requires endomyocardial biopsy (EMB) for a definite diagnosis—is often misdiagnosed as other, more common, causes of left ventricular "hypertrophy" (LVH), including hypertensive heart disease and hypertrophic cardiomyopathy (HCM) (1). We (2,3) and other groups (4,5) have previously documented that ^{99m}Tc-3,3-diphosphono-1,2-propanodicarboxylic acid (^{99m}Tc-DPD) has a high affinity for TTR-infiltrated myocardium (allowing a differential diagnosis with light-chain [AL] cardiac amyloidosis, in which the tracer uptake is low/absent) (2,3). However, the scintigraphic profiles of the non–amyloidotic cardiomyopathies potentially mimicking SSA are not known, and the

specificity of ^{99m}Tc-DPD for the diagnosis of SSA in this context remains to be ascertained. To clarify this aspect, we retrospectively analyzed a group of consecutive patients with suspected SSA studied at our center, according to a pre-defined echocardiographic-scintigraphic-genetic and EMB protocol.

We considered all patients who underwent ^{99m}Tc-DPD scintigraphy from 2004 to 2011 for suspected SSA, that is, patients older than 65 years-of-age with unexplained concentric LVH (end-diastolic mean wall thickness >13 mm) and a nondilated left ventricle (LV), also presenting 1 or more of the following: male sex; thickened interatrial septum; thickened atrioventricular valves; mild pericardial effusion; granular sparkling appearance; and absent/mild LVH on the electrocardiogram (ECG). We excluded patients with a known definite diagnosis that explained LVH, including AL amyloidosis, hereditary TTR-related amyloidosis (ATTR), and sarcomeric HCM.

Patients received 740 MBq of ^{99m}Tc-DPD intravenously. Whole-body scans were obtained at 5 min (early) and 3 h (late) after injection. Visual score of cardiac retention was: 0, absent cardiac uptake, normal bone uptake; 1, mild cardiac uptake, inferior to bone uptake; 2, moderate cardiac uptake, attenuated bone uptake; and 3, strong cardiac uptake, mild/absent bone uptake (2,3). Heart retention (HR), whole-body retention, and heart/whole-body retention ratio (H/WB) were semiquantitatively assessed using a standard region-of-interest technique (2–4). Total counts in the scans were taken as whole-body counts. Early whole-body counts were assumed to represent total injected activity. Whole-body retention was evaluated by comparing counts in late images (after subtraction of counts in the bladder and urinary tract, and correction for decay and scan speed) with those in early whole-body images. HR was evaluated by comparing decay-corrected counts of the heart in late images with counts in early whole-body images. H/WB ratios were calculated by dividing counts in the heart by whole-body counts in late images.

Sixty-seven patients were included. Data are expressed as numbers and percentages or median value and [interquartile range]. Visual ^{99m}Tc-DPD myocardial uptake was present (positive) in 51 patients (all with a visual score ≥2) and absent (negative) in 16 (visual score = 0). EMB (including histological and immunohistochemical evaluation) was performed in 46 of 51 patients with

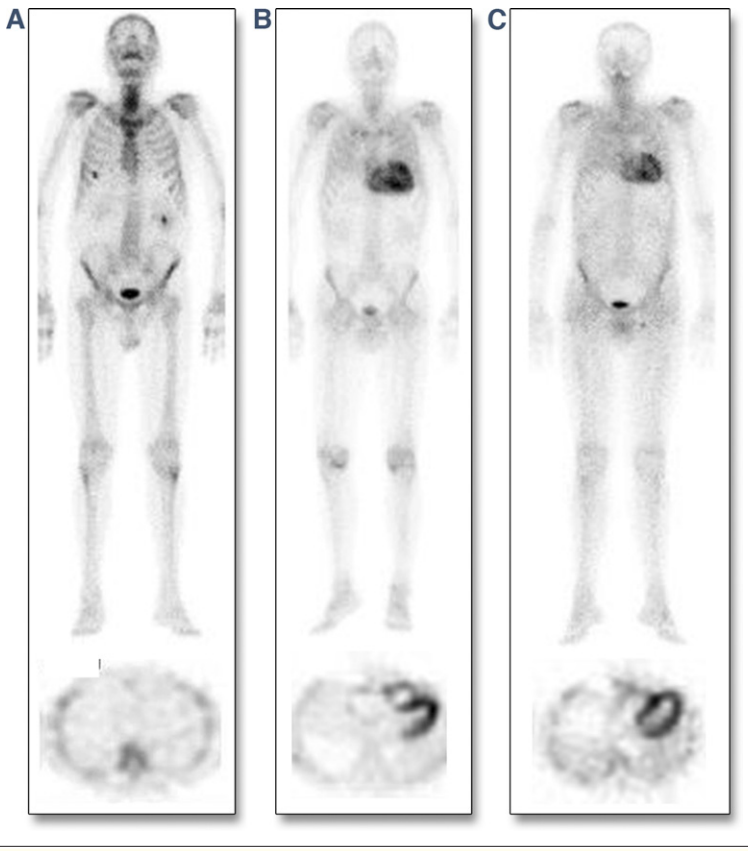

Figure 1. Representative Examples of ^{99m}Tc-DPD Scintigraphy in SSA, ATTR, and HCM

Examples illustrating the spectrum of ^{99m}Tc-3,3-diphosphono-1,2-propanodicarboxylic acid (^{99m}Tc-DPD) uptake among patients with transthyretin (TTR)-related (senile systemic amyloidosis [SSA] or hereditary TTR-related amyloidosis [ATTR]) amyloidotic cardiomyopathy or other non–amyloidotic cardiomyopathies (**top row** = whole-body scans, anterior view; **bottom row** = cross-sectional views of cardiac single-photon emission computed tomography in the same patients). **(A)** Patient with sarcomeric hypertrophic cardiomyopathy (HCM) without any visually detectable myocardial tracer uptake (visual score = 0). **(B, C)** Two patients with TTR-related amyloidosis (patient B affected by SSA, patient C affected by ATTR), both showing strong myocardial ^{99m}Tc-DPD uptake and attenuated bone uptake of the tracer.

positive scintigraphy (5 patients refused EMB) and documented TTR-related amyloid infiltration in all cases. At deoxyribonucleic acid analysis, TTR mutations were present in 14 patients (leading to a diagnosis of ATTR) and absent in 32 (leading to a diagnosis of SSA). No TTR mutations were found in the 16 patients with negative scintigraphy: 9 were found to carry sarcomeric gene mutations (*MYBPC3* in 5 cases, *MYH7* in 4 cases), leading to a diagnosis of HCM; a single patient was found to carry an alpha-galactosidase A gene mutation, leading to a diagnosis of Anderson-Fabry disease. The remaining 6 patients (without genetic abnormalities) underwent EMB, which documented only a mild nonspecific hypertrophy without myocardial disarray, supporting a diagnosis of hypertensive heart disease. In this way, 3 groups of patients with different diagnoses were identified: SSA, ATTR, and non–amyloidotic cardiomyopathies. Figures 1 and 2, respectively, show examples of individual scintigraphic profiles and median values of HR and H/WB in the 3 groups.

Clinically, 17 (53%) SSA and 7 (50%) ATTR patients were initially referred for heart failure, the other patients for atrial fibrillation or occasional finding of ECG/echocardiographic abnormalities. The 16 cases with non–amyloidotic LVH were initially referred for "diastolic heart failure" (n = 3, 19%), atrial fibrillation (n = 4, 25%), or occasional finding of ECG/echocardiographic abnormalities (n = 9, 56%). SSA patients were older (78 [74 to 81] years) than ATTR patients (69 [67 to 71] years) and patients with non–amyloidotic LVH (67 [66 to 70] years, $p < 0.001$). Male sex was predominant in all groups (91% in SSA, 100% in ATTR, 75% in non–amyloidotic LVH; p = 0.10). A concomitant carpal tunnel syndrome was present in 6 (46%) ATTR patients, 7 (22%) SSA patients, and 1 patient with non–amyloidotic LVH (p = 0.06). Low QRS voltage was present in 11 (34%) SSA patients, 6 (43%) ATTR patients, and 2 (13%) patients with non–amyloidotic LVH (p = 0.15).

Echocardiographically, despite a similar interventricular septal thickness (18 [16 to 20] mm in all groups), LV posterior wall thickness was higher among SSA (18 [15 to 19] mm) and ATTR (17 [15 to 19] mm) patients compared with those with non–amyloidotic LVH (14 [13 to 15] mm, p = 0.004). Interatrial septum thickening was more frequent in SSA (63%) and ATTR patients (57%) than in those with non–amyloidotic LVH (25%, p = 0.04). Atrioventricular valve thickening was more prevalent in ATTR patients (64%) than SSA patients (50%) and patients with non–amyloidotic LVH (19%, p = 0.03). Pericardial effusion was present in 14 (44%) SSA patients, 4 (28%) ATTR patients, and 3 (19%) patients with non–amyloidotic LVH (p = 0.2). LV ejection fraction was normal in non–amyloidotic LVH (68% [64% to 70%]), and within the lower normal limits or mildly reduced in patients with SSA (50% [35% to 59%]) and ATTR (50% [38% to 52%]).

Using genotyping/immunohistochemistry as the reference technique, the sensitivity and specificity of a myocardial ^{99m}Tc-DPD visual score ≥2 for the diagnosis of TTR-related cardiomyopathy were both 100%. All other clinical, echocardiographic, and electrocardiographic findings showed lower sensitivity and specificity values: respectively, 94% and 25% for male sex, 28% and 94% for carpal tunnel syndrome, 61% and 75% for interatrial septum thickening, 37% and 81% for atrioventricular valve thickening, 39% and 81% for pericardial effusion, and 37% and 88% for ECG low QRS voltage. When interpreting these values, one must consider the high "pre-test" probability of SSA in the study population—due to the accurate patient pre-selection—and the fact that in all positive cases, tracer uptake was intense (visual score ≥2). Indeed, as our previous studies showed, a visual score ≤2 is possible in AL amyloidotic cardiomyopathy.

Our study, which considered an accurately selected population with a high prevalence of non–AL amyloidotic cardiomyopathy, shows that in elderly patients with unexplained concentric LVH and a nondilated LV, ^{99m}Tc-DPD scintigraphy can provide a valuable, accurate (and inexpensive) technique, able to increase the possibility of noninvasive identification of TTR-related amyloidotic cardiomyopathies on top of echocardiographic evaluation. This can be particularly useful for the noninvasive identification of SSA (for

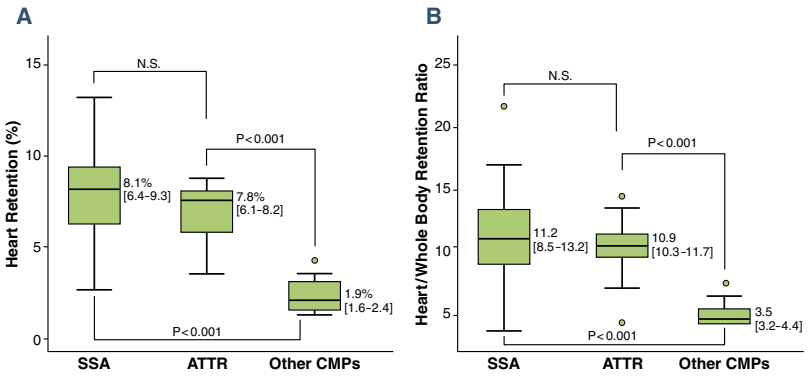

Figure 2. ^{99m}Tc-DPD Heart Retention and Heart/Whole-Body Retention Ratio in Patients With SSA, ATTR, or HCM

Comparison of ^{99m}Tc-DPD heart retention **(A)** and heart/whole-body retention ratio **(B)** between patients with TTR-related amyloidotic cardiomyopathy (SSA and ATTR) and patients with other non–amyloidotic cardiomyopathies (other CMPs). Lower/upper limits of the boxes indicate 25th/75th percentiles; **horizontal lines** within boxes indicate medians. **Circles** represent outliers (values lying more than 1.5 interquartile range outside the 25th or the 75th centile). Abbreviations as in Figure 1.

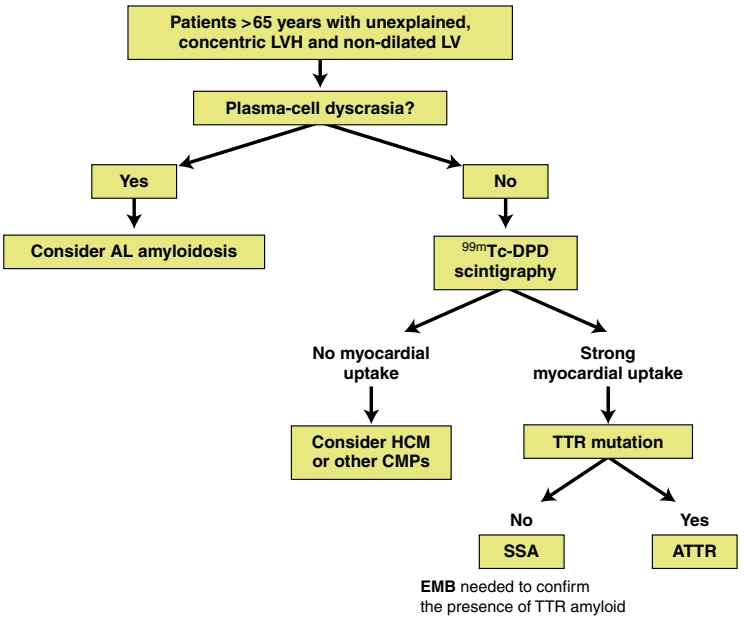

Figure 3. Role of ^{99m}Tc-DPD Scintigraphy in the Diagnostic Workup

Proposed clinical application of ^{99m}Tc-DPD in elderly patients with an echocardiographic profile of unexplained, concentric left ventricular hypertrophy (LVH) and a nondilated left ventricle (LV). Once a plasma-cell dyscrasia has been excluded, ^{99m}Tc-DPD scintigraphy could be useful in identifying patients with TTR-related cardiac amyloidosis (strong myocardial visual uptake of ^{99m}Tc-DPD) and patients with non–amyloidotic cardiomyopathies (CMPs, absent myocardial visual uptake of ^{99m}Tc-DPD). The differential diagnosis between SSA and ATTR requires deoxyribonucleic acid analysis. AL = light-chain; EMB = endomyocardial biopsy; other abbreviations as in Figures 1 and 2.

which, differing from ATTR, there is no genetic diagnostic standard) (Fig. 3).

Candida Cristina Quarta, MD, Pier Luigi Guidalotti, MD, Simone Longhi, MD, Cinzia Pettinato, MD, Ornella Leone, MD, Alessandra Ferlini, MD, Elena Biagini, MD, Francesco Grigioni, MD, Maria Letizia Bacchi-Reggiani, MSc, MStat, Massimiliano Lorenzini, MD, Agnese Milandri, MD, Angelo Branzi, MD, Claudio Rapezzi, MD*

*Istituto di Cardiologia, Policlinico S. Orsola-Malpighi, via Massarenti 9, 40138 Bologna, Italy. *E-mail: claudio.rapezzi@unibo.it.*

http:dx.doi.org/10.1016/j.jcmg.2012.02.015

REFERENCES

1. Falk RH, Dubrey SW. Amyloid heart disease. Prog Cardiovasc Dis 2010;52:347–61.
2. Perugini E, Guidalotti PL, Salvi F, et al. Noninvasive etiologic diagnosis of cardiac amyloidosis using ^{99m}Tc-3,3-diphosphono-1,2-propanodicarboxylic acid scintigraphy. J Am Coll Cardiol 2005;46:1076–84.
3. Rapezzi C, Quarta CC, Guidalotti PL, et al. Usefulness and limitations of ^{99m}Tc-3,3-diphosphono-1,2-propanodicarboxylic acid scintigraphy in the aetiological diagnosis of amyloidotic cardiomyopathy. Eur J Nucl Med Mol Imaging 2011;38:470–8.
4. Puille M, Altland K, Linke RP, et al. ^{99m}Tc-DPD scintigraphy in transthyretin-related familial amyloidotic polyneuropathy. Eur J Nucl Med Mol Imaging 2002;29:376–9.
5. Kristen AV, Haufe S, Schonland SO, et al. Skeletal scintigraphy indicates disease severity of cardiac involvement in patients with senile systemic amyloidosis. Int J Cardiol 2011 Jul 15 [E-pub ahead of print].

Myocardial Imaging for Mitochondrial Membrane Potential

The editorial by Strauss and Schoder (1) indicates that all useful myocardial perfusion tracers, regardless of chemical structure, mechanism of uptake, and retention, follow the Sapirstein principle, even when, save perhaps for ^{15}O-water, they actually fail to conform to the essential requirement postulated by Sapirstein (2) for such a tracer; namely, first-pass extraction fraction of 1. The editorial goes on to state that such tracers ". . . still provide accurate measurements of regional and *absolute* [emphasis added] perfusion and perfusion reserve if imaging is performed before significant loss of indicator from the tissue" (1). We performed an additional analysis of the data pertinent to the relationship between 4-[18F]-Tetraphenylphosphonium (18F-TPP) measurement of absolute myocardial blood flow (MBF) and corresponding microsphere measurements of absolute MBF under conditions of adenosine stimulation with phenylephrine support (Fig. 1) to further address the issue raised by Strauss and Schoder (1) in their editorial.

In brief, we used all the ex vivo tissue samples (n = 112) from all the animals (n = 6) reported in our study (3). Each myocardial sample had a microsphere measurement of absolute MBF and a well counter determined measure of 18F-TPP concentration. We modified slightly the method of Di Rocco et al. (4) to compute